



LETTER • OPEN ACCESS

Controls on coastal saline groundwater across North America

To cite this article: Daniel V Kretschmer et al 2025 Environ. Res. Lett. 20 024065

View the article online for updates and enhancements.

You may also like

- Identification of freshwater saltwater interface in coastal areas using combination of geophysical and geochemical methods: A case study in Mekong Delta, Vietnam Quang-Khai Ha, Phu Le Vo, Chu-Nam Phan et al.
- A model comparison assessing the importance of lateral groundwater flows at the global scale
- Inge E M de Graaf and Kerstin Stahl
- Frequency Analysis on Groundwater Consumption and Water Billed to the Community in Kelantan Nur Aqilah Fatini Che Ayob and Sabariah



ENVIRONMENTAL RESEARCH

LETTERS



OPEN ACCESS

RECEIVED

25 October 2024

REVISED

4 January 2025

ACCEPTED FOR PUBLICATION

13 January 2025

PUBLISHED

7 February 2025

Original content from this work may be used under the terms of the Creative Commons Attribution 4.0 licence.

Any further distribution of this work must maintain attribution to the author(s) and the title of the work, journal citation and DOI.



LETTER

Controls on coastal saline groundwater across North America

Daniel V Kretschmer^{1,2,*}, Holly A Michael³, Nils Moosdorf^{1,5}, Gualbert H P Oude Essink^{6,7}, Marc F P Bierkens^{6,7}, Thorsten Wagener² and Robert Reinecke^{1,2}

- Institute of Geography, Johannes Gutenberg-University Mainz, Mainz, Germany
- ² Institute of Environmental Science and Geography, University of Potsdam, Potsdam, Germany
- ³ Department of Earth Sciences, University of Delaware, Newark, DE, United States of America
- ⁴ Leibniz Centre for Tropical Marine Research (ZMT), Bremen, Germany
- ⁵ Institute of Geosciences, University of Kiel, Kiel, Germany
- ⁶ Unit Subsurface and Groundwater Systems, Deltares, Utrecht, The Netherlands
- Department of Physical Geography, Utrecht University, Utrecht, The Netherlands
- * Author to whom any correspondence should be addressed.

E-mail: dkretsch@uni-mainz.de, hmichael@udel.edu, nils.moosdorf@leibniz-zmt.de, gualbert.oudeessink@deltares.nl, m.f.p.bierkens@uu.nl, thorsten.wagener@uni-potsdam.de and reinecke@uni-mainz.de

Keywords: groundwater salinity, continental groundwater model, variable densities, groundwater model, coastal zone Supplementary material for this article is available online

Abstract

Groundwater is crucial to sustaining coastal freshwater needs. About 32 million people in the coastal USA rely on groundwater as their primary water source. With rapidly growing coastal communities and increasing demands for fresh groundwater, understanding controls of continental-scale coastal groundwater salinity is critical. To investigate what hydrogeological factors (e.g. topography, hydraulic conductivity) control coastal saline groundwater at continental scales, we have simulated variable-density groundwater flow across North America with the newly developed Global Gradient-based Groundwater Model with variable Densities (G³M-D). The simulation results suggest that under a steady climate and pre-development conditions (i.e. steady 30-year mean groundwater recharge, no withdrawals nor sea level rise) saline groundwater is present in 18.6% of North America's coastal zone, defined as up to 100 km inland and up to 100 m above mean sea level. We find that the coastal zone is particularly vulnerable to containing saline groundwater at low hydraulic gradients ($<10^{-4}$) and large hydraulic conductivities $(>10^{-2} \text{ m d}^{-1})$. To analyze model parameter sensitivities, i.e. which parameters control the resulting distribution of saline groundwater, we utilize the inherent spatial model variability. We find that hydraulic gradient, topographic gradient, hydraulic conductivity, and aquifer depth are important controls in different places. However, no factor controls coastal groundwater salinization alone, suggesting that parameter interactions are important. Using G³M-D based on G³M, a model that previous work found to be strongly controlled by topography, we find no controlling influence of recharge variability on the saline groundwater distribution in North America. Despite a likely overestimation of saline interface movement, the model required 492 000 years to reach a near-steady state, indicating that the saline groundwater distribution in North America has likely been evolving since before the end of the last ice age, approximately 20 000 years ago.

1. Introduction

Coastal groundwater is vital to sustaining coastal freshwater consumption and agricultural activities in the US (Barlow and Reichard 2010) and other countries worldwide (Custodio 2010, Shi and Jiao 2014, Manivannan and Elango 2019). About half of

all coastal counties (143 of 297) in the US, home to 32 million people, rely on groundwater as their main water supply (Dieter *et al* 2018) Between 1960 and 2008, the population in coastal counties in the US grew by over 80%, 20% more than non-coastline counties (Wilson and Fischetti 2010). Over a similar period, from 1950 to 2015, the growing demand for

freshwater led to a doubling of groundwater withdrawal in the US (Dieter *et al* 2018), causing hydraulic gradients at the coast to reduce and even turn landward (Jasechko *et al* 2020).

Where hydraulic gradients at the coast decline (e.g. due to a drop in the groundwater table or relative to sea level rise), saline ocean water may intrude into the groundwater system and salinize freshwater aquifers. In addition to growing water demand, storm surges and sea-level changes may exacerbate seawater intrusion (Post et al 2018). Seawater intrusion has already affected coastal groundwater across North America (Barlow and Reichard 2010). Worldwide, nearly a third of all coastal metropolises are threatened by seawater intrusion (Cao et al 2021). However, our understanding of the rapidly changing coastal groundwater lacks predictive capabilities (Richardson et al 2024), which is why we need to better understand dominant controls of coastal saline groundwater and how these vary along coastlines.

Several continental and global studies have addressed the issue of seawater intrusion. In a study of the US coast, Ferguson and Gleeson (2012) show that groundwater withdrawal in coastal regions is a greater control on horizontal seawater intrusion than sea level rise or changes in groundwater recharge (GWR). Based on estimated submarine groundwater discharge and groundwater withdrawals, 9% of the contiguous United States coastline are vulnerable to seawater intrusion (Sawyer et al 2016). Resilience against seawater intrusion driven by sea level rise is higher when groundwater levels within aquifers can shift upwards, balancing the gradient change induced by sea level rise (Michael et al 2013). In other words, aguifers are more resilient where the topographic gradient to the coast remains larger than the hydraulic gradient to the coast as sea-level rise progresses. Similarly, groundwater simulations along the coast of California show that coastal topography controls seawater intrusion and overland flooding due to sea-level rise (Befus et al 2020). Recently published results from groundwater models in 1200 coastal regions around the world suggest that coastal fresh groundwater volumes will decrease by about 5% until 2100 due to sea-level rise (Zamrsky et al 2024). They confirmed previous findings showing higher resilience against seawater intrusion in regions with higher topographic gradients, often aligning with steeper hydraulic groundwater gradients.

However, previous simulations of coastal ground-water share a major limitation: their model extent is limited landward, thus requiring assumptions about the landward boundary condition (Michael *et al* 2013, Zamrsky *et al* 2024), which can strongly impact the results of seawater intrusion simulations (Werner and Simmons 2009, Ketabchi *et al* 2016). Michael *et al* (2013) simulated a theoretical aquifer to analyze

the effect of changing GWR, hydraulic conductivity, and anisotropy on the saltwater distribution in the aquifer. However, since the changes were applied one at a time, their combined effects were not simulated. Further, the only global assessment of seawater intrusion (Zamrsky et al 2024) was limited to a quarter of the global coastline with permeable unconsolidated sedimentary formations. Hence, wide parameter ranges and combinations remain unexplored. Table S1 shows a comparison of continental and global coastal groundwater models.

Here, we use a Darcy approach (Reinecke et al 2019b) to simulate groundwater flow of the entire North American continent under a steady climate (e.g. steady GWR) and natural, pre-pumping conditions (i.e. without withdrawals). The density zones are simulated with a SWI2-like variable density routine (Bakker et al 2013). Like the problem described by Henry (1964), the entire groundwater system is fresh in its initial state, ensuring that the ocean is the only source of saltwater (which is a simplification as saline groundwater can have multiple other sources). As the over 450 000 model cells were parameterized individually, the model incorporates all combinations of input parameters existing at the simulated resolution of 5 arcminute (roughly 9.2 km at the Equator). This allows us to assess which of the impact factors, topographic gradient (dT), hydraulic gradient (dH), hydraulic conductivity (K), aquifer depth (D_{aqu}), and groundwater recharge (GWR) control the simulated distribution of saline groundwater.

2. Methods

2.1. The global gradient-based groundwater model The global gradient-based groundwater model, G³M

(Reinecke *et al* 2019a, 2019b), was inspired by concepts of MODFLOW-2005 (Harbaugh *et al* 2005) and built to be coupled with global hydrological models. To facilitate the assessment of groundwater at the global scale, hydraulic gradients between grid cells drive the flow between the cells. The three-dimensional flow of groundwater is described by a partial differential equation (Harbaugh *et al* 2005):

$$\frac{\partial}{\partial x} \left(K_{xx} \frac{\partial h}{\partial x} \right) + \frac{\partial}{\partial y} \left(K_{yy} \frac{\partial h}{\partial y} \right) + \frac{\partial}{\partial z} \left(K_{zz} \frac{\partial h}{\partial z} \right)$$

$$+ W = S_s \frac{\partial h}{\partial t}$$

where K_{xx} , K_{yy} , and K_{zz} [LT⁻¹] are the hydraulic conductivities along the x, y, and z axes between the cells with sizes Δx , Δy , and Δz [L]; S_s [L⁻¹] is the specific storage; h [L] is the hydraulic head. W [T⁻¹] incorporates the flows into and out of each cell, such as GWR, surface water bodies (i.e. rivers, lakes, and wetlands), or the ocean. Just like the flows between the

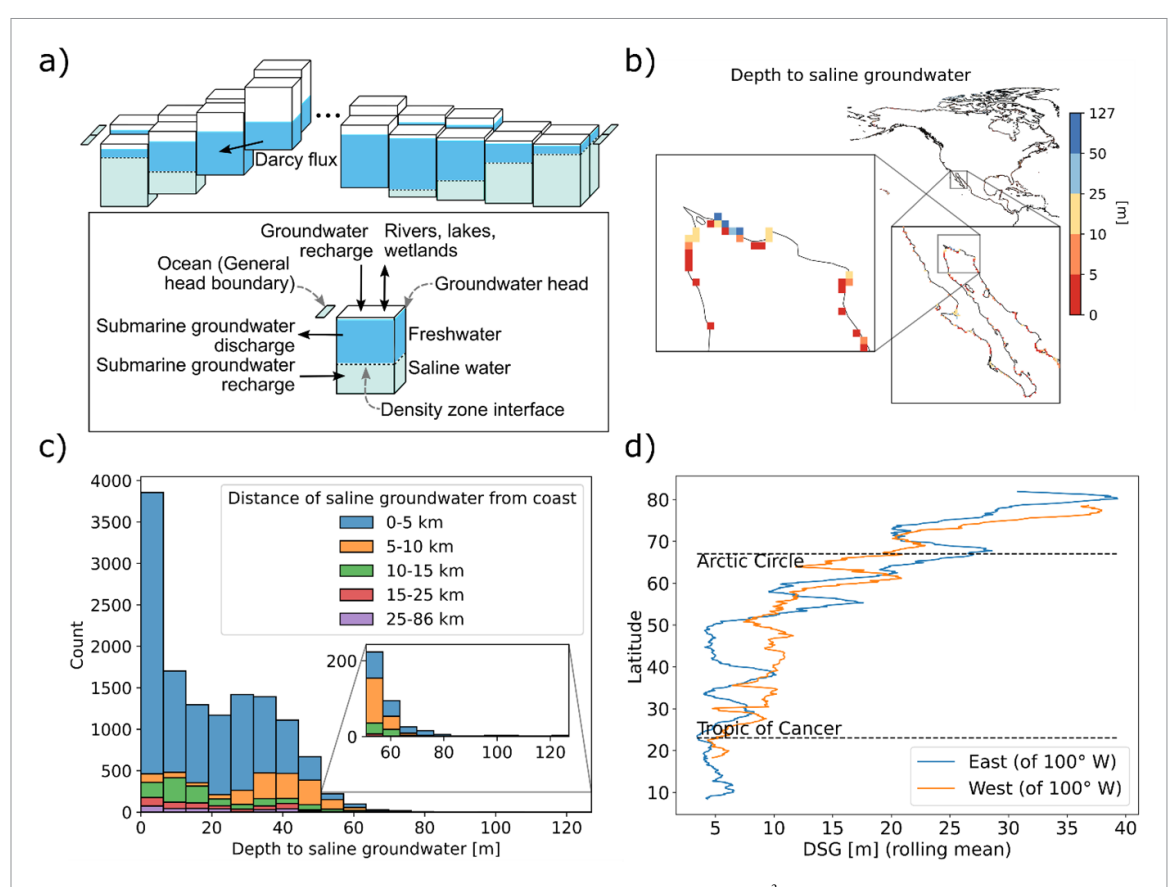


Figure 1. Panel showing (a) the concept of the variable density groundwater model (G^3M -D), (b) simulated depth to saline groundwater (DSG) at Baja California (for the entire map of North America, see figure S1), (c) a histogram of simulated depths to saline groundwater, and (d) the moving average of DSG on the east and west coast of North America by latitude (separation at 100° W). The model cell size is 5 arcminute (\sim 9.2 km at the equator).

cells, the flow from a cell to a river, lake, wetland, or ocean depends on the respective heads. Thus, each cell can receive/give water from/to neighboring cells and additionally from/to rivers, lakes, wetlands, and the ocean. In a coupled state, these surface water bodies are updated by the hydrological model. In this study, surface water heads are kept at their initial elevation (30th percentile of a 30 arcsecond digital elevation model; Reinecke *et al* 2019b).

2.2. The added variable density routine

Freshwater has a lower density than saline water. In the newly developed Global Gradient-based Groundwater Model with variable Densities (G³M-D), sharp interfaces lie between density zones representing salinity levels. The height of these interfaces is simulated similarly to the Saltwater Intrusion package (SWI2) developed for MODFLOW (Bakker *et al* 2013). A SWI2-like routine was implemented due to its wide range of applications and low simulation cost, which are essential in developing large-scale models. Compared to G³M, which simulates groundwater heads, G³M-D has an additional density interface routine. The groundwater head routine accounts for the density zone volumes in each cell before solving

the variable density equations in the separate density interface routine. Hence, the mass balance equation (used with constant density) is replaced by a volume balance equation when simulating variable densities (text S1 and Bakker *et al* 2013). As density interfaces may need many time steps to develop, multiple shorter variable density time steps can be simulated per groundwater flow step to reduce simulation time.

2.2.1. Density zones and density interfaces

In G³M-D, like in SWI2, density zones in each cell are stacked vertically (see figure 1(a)). The model calculates the height of horizontal sharp density interfaces, representing the limits of density zones. Each zone is constant in density (i.e. this corresponds to the discontinuous option in SWI2). In a setup with one density interface between the two density zones of freshwater and seawater (used in this study), the density interface represents the approximate location of 50% seawater in the aquifer, neglecting the effects of dispersion and diffusion. In other words, density interface heights change when the proportions of density zones within a cell change, without simulating a mixing of density zones. Another limitation is that density can only be inverted between model layers

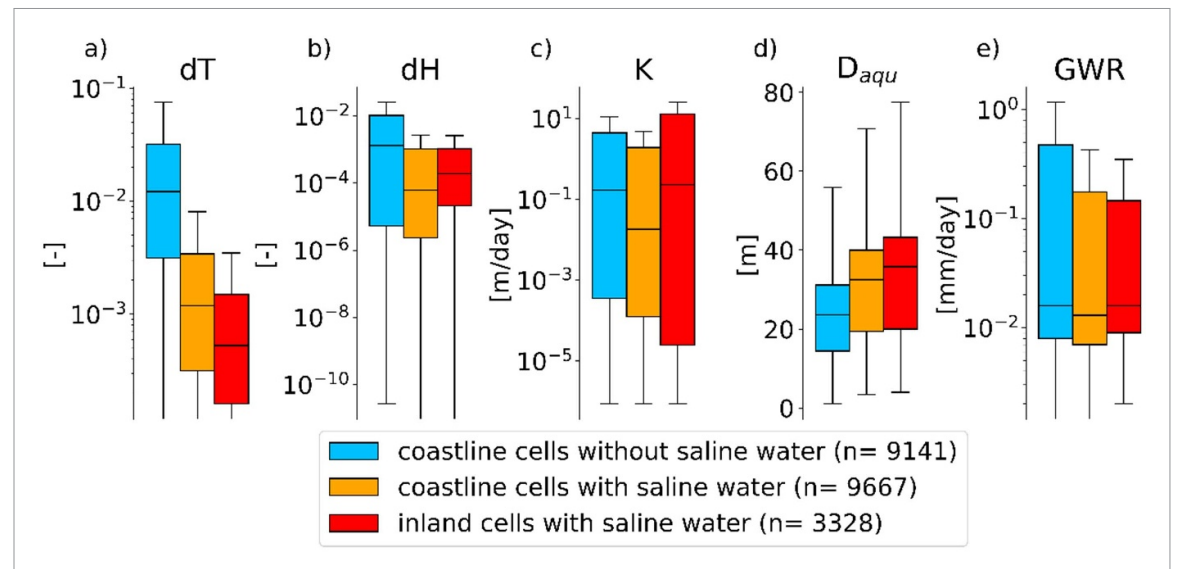


Figure 2. Boxplots of (a) topographic gradient (dT), (b) hydraulic gradient (dH), (c) hydraulic conductivity (K), (d) aquifer depth (D_{aqu}) , and (e) groundwater recharge (GWR) in coastline cells (i.e. cells with one side facing an ocean) without saline groundwater (blue), coastline cells with saline groundwater (orange), and inland cells with saline groundwater (red). Subplots (a), (b), (c) and (e) are in logarithmic scale and hence do not show 0 on the *y*-axis (see figure S6 for plot without logarithmic scales).

(i.e. aquifers) but not within the same model layer. At each density time step, new interface heights are computed iteratively for all cells with saline water, followed by interface adjustments. These adjustments allow the horizontal movement of saline water from a cell with saline water to an entirely fresh neighboring cell (e.g. when the slope between a density interface and the neighboring cell bottom is above a threshold). For equations and subroutines of the density routine, please refer to text S1 and Bakker *et al* (2013).

2.2.2. Model mechanisms

While freshwater inputs (i.e. from GWR, rivers, or neighboring cells) into a cell may increase the groundwater head, inputs of saline water (i.e. inflow from the ocean or a neighboring cell) may also cause a rise in density interfaces. At the coast, G³M-D incorporates several mechanisms determining the salinity distribution (figure S2). Similar to the Ghyben–Herzberg relation, elevated freshwater heads may induce a flow of saline water out of the cell, lowering the density interface height. Thus, steep terrain (high dT), which can come with high freshwater levels (i.e. if hydraulic conductivity if low and recharge is high), may lead to low saline water levels (figures S2(a) and (b)). Additionally, if the aquifer depth does not increase significantly towards inland, steep terrain can result in bottoms of cells located higher than their neighboring cell's saline zones, stopping further salinization. Thus, saline water may reach further inland in flat (low dT) terrain than in steep terrain (figures S2(a) and (b)). (Figures S2(c) and (d)) show that in coastline cells with low aquifer depth, low cell surface elevation can disconnect the cell from the ocean, prohibiting salinization. Meanwhile, higher aquifer depths

allow salinization even for higher surface elevation of the coastline cell (figures 2(e) and (f))). Groundwater levels in cells with low GWR are lower than in cells with high GWR. The smaller freshwater column in cells with low GWR allows saline water to intrude further (figures S2(f) and (g)). Cells with high hydraulic conductivity drain quicker and thus may have lower fresh groundwater levels than cells with low hydraulic conductivity. The lower fresh groundwater levels in cells with high hydraulic conductivity may result in further intrusion of saline groundwater (figures S2(h) and (i)).

2.2.3. Testing the implementation

The newly implemented variable density routine was tested using Examples 1–3 from the SWI2 documentation (Bakker *et al* 2013). Each example tests different parts of the implementation (see figure S3). The results of Example 1 show that G³M-D can accurately simulate the height change of one density interface in an aquifer with an inflow of saline water. Example 2 shows that more than one interface can be simulated correctly, simulating two interfaces rotating around the brackish zone they enclose. Including three different aquifer layers with changing hydraulic conductivities, Example 3 demonstrates that the movement of a density interface between layers is also accurate.

2.3. The variable-density groundwater model of North America

2.3.1. Model setup

Several global datasets are used in the G³M-D model setup of the North American continent, including the entire inland. Elevation and surface water bodies (i.e. rivers, lakes, and wetlands) are parameterized as in Reinecke *et al* (2019b). GLHYMPS 2.0

Table 1. Aspects of coastal saline groundwater with their respective abbreviations and explanations.

Aspect of coastal saline groundwater	Abbreviation	Calculated as	Aspect pronounced if
Saline groundwater fraction	SGF	Share of saline water in the groundwater column	SGF > 0.5
Thickness of fresh groundwater column	TFG	Groundwater head—interface height in meters	TFG < 5 m
Distance of saline groundwater from coast	DC	Cell distance from the coastline in kilometers	DC > 10 km

(Huscroft et al 2018) provided hydraulic conductivity (mean of model cells: 8.57 m d⁻¹) and effective porosity (mean of model cells: 0.047). Cells with an effective porosity of 0 (56% of the model cells, 20.4% at the coastline) are excluded from the variable density routine, meaning they cannot hold saline water. The model does not represent conduits (e.g. in karstic or volcanic aquifers). The GWR input was calculated as the 1987-2016 mean from a WaterGAP (Müller Schmied et al 2020) simulation using WFDEI (Weedon et al 2014) as meteorological forcing (mean of model cells: 0.187 mm d^{-1}). The thickness of the single aquifer layer was defined using depth to bedrock data (mean of model cells: 24.26 m) by Shangguan et al (2017). This entails that no aquitards or deep confined aquifers are represented in the model. The input data for elevation, GWR, effective porosity, hydraulic conductivity, and aquifer thickness are displayed in figure S3.

A general head boundary (GHB) (Harbaugh 2005) represents the ocean at all coastline cells and is set to a constant elevation of 0 m. The coastal shoreline permeability was retrieved from the global coastal permeability dataset (CoPerm) (Moosdorf et al 2024) and used to parameterize the GHB conductance. No groundwater pumping was included in the simulation to assess the coastal saline groundwater under naturalized conditions. The assumption that the ocean is the only source of saltwater entails that existing saline groundwater deposits in large parts of North America are omitted (Feth 1965, Reilly et al 2008). Two density zones are simulated in the presented model configuration—freshwater and saline water (stemming from the ocean). Assuming a constant groundwater temperature of 12 °C for the entire North American continent, freshwater (salinity: 0 parts per thousand) was assigned the density of 999.5 kg m $^{-3}$, and ocean water (salinity: 35 parts per thousand) was assigned the density of 1026.6 kg m $^{-3}$. A comparison to other continental or global studies on coastal saline groundwater is shown in table S1.

2.3.2. Finding stable interface positions

At the start of the simulation, all groundwater in the system was fresh. Over time, saline ocean water intruded the simulated system through the GHB. Since groundwater density develops significantly slower than the groundwater head, the model was run under pseudo-steady state conditions (Bakker et al 2013), i.e. with steady sea level, coastline, and recharge, while computing changes in density interface heights. Further, one thousand annual density time steps were simulated for each groundwater flow time step of thousand years. The simulation was run until the interface heights were stable, i.e. the following conditions were satisfied: in two consecutive time steps of thousand years the interface height change (a) in 95% of the cells with saline water is below 0.05 m and (b) in 99% of the cells with saline water was below 0.1 m. This was the case after 492 time steps (i.e. 492 000 years).

2.4. Utilizing spatial variability of inputs and outputs to understand process controls

The groundwater model of North America simulates heads and interface heights in 452 736 cells, of which 18 808 are coastline cells (i.e. cells with at least one side facing the ocean). We use the intrinsic spatial variability of inputs and outputs in our evaluation to analyze the factors that control coastal saline groundwater (similar to Gnann *et al* 2023). We consider three aquifer properties: aquifer depth, hydraulic conductivity, and topographic gradient, as well as two hydrologic characteristics: GWR and the hydraulic gradient (resulting from the groundwater head routine).

For all cells containing saline groundwater at the stable state, we evaluate three different aspects of coastal saline groundwater: saline groundwater fraction (SGF), thickness of fresh groundwater (TFG) column, and distance of saline groundwater from coast (DC) (table 1). We separately assess factor value distributions in cells with moderate and pronounced (1) SGF, (2) TFG column, and (3) distance

of saline groundwater from the coast to assess which factors control the severity of saltwater occurrence in coastal groundwater (see table 1). We repeated this evaluation with increased and decreased thresholds to assess the sensitivities of the thresholds separating into moderate and pronounces aspects of coastal saline groundwater.

To assess the simulated saline groundwater distribution, we use the salinity observations dataset by Thorslund and van Vliet (2020). All observations within the boundaries of grid cells were assigned the factor values (e.g. dH, K) of that cell. The observations were classified into saline and fresh using a threshold for electrical conductivity. If an observation has an electrical conductivity above 800 μ S cm⁻¹, it was categorized as saline.

3. Results

In the final (stable) state of the salinity interfaces, 12 995 (2.9%) of the 452 736 simulated cells contained saline groundwater (9667 of which were coastline cells). The simulated state does not necessarily represent the current real-world situation. It evolved from an initial entirely fresh groundwater system and shows the potential spatial distribution of saline groundwater for steady GWR and sea level without groundwater pumping or historical marine brine deposits. The simulated depth to saline groundwater (DSG) in most cells (86%) containing saline water is less than 40 m (figure 1(c)), with large regions of shallow saline groundwater in Alaska (US), Nunavut (Canada), and Oaxaca (Mexico) (figure 1(b)) and S4). In both the east and west of North America, DSG reduces from about 50 m in the north to roughly 10 m in the south (figure 1(d), reflecting the aquifer thickness distribution (figure S4). In the following, we examine the sensitivity to the possible impacting factors, i.e. topographic gradient (dT), hydraulic gradient (dH), hydraulic conductivity (K), aquifer depth (D_{aou}) , and groundwater recharge (GWR) to find the dominant controls in coastal groundwater salinity on the continental scale.

3.1. Topographic gradient and aquifer depth control incursion at the continental coastline

Roughly half (i.e. 9667 of 18 808) of the North American coastline cells (i.e. cells with at least one side facing the ocean) contain saline water in the stable state, while the other half (9141) stays entirely fresh. Figure 2 shows the factor distributions of (1) coastline cells without saline water (blue), (2) coastline cells with saline water (orange), and (3) inland cells with saline water (red). Fresh inland cells are omitted in figure 2. The median topographic gradient (dT) in coastline cells without saline water (just over 0.02) is one order of magnitude larger than

in coastline cells with saline water (just over 0.002) (figure 2(a)), mainly because saline water can only enter a model cell if the sea level is above the aquifer bottom (applies to 66% of coastline cells). The median hydraulic gradient (dH) in coastline cells without saline water (roughly 10^{-3}) is one order of magnitude larger than in cells with saline groundwater at the coastline and inland (figure 2(b)). Besides topographic gradient (dT), hydraulic conductivity (*K*) seems to control the distribution of saline water inland, since hydraulic conductivity is much higher in inland cells containing saline water (figure 2(c)). Further, cells with saline water tend to have a larger aquifer depth (figure 2(d)) and GWR can be much higher in fresh coastline cells than in cells with saline groundwater (figure 2(e)).

3.2. Several factors control coastal groundwater salinity at the continental scale

We apply thresholds (table 1) to categorize SGF, the TFG column, and the distance of saline groundwater from the coast (DC) into moderate and pronounced to assess which parameters control the severity of an aspect of coastal saline groundwater in a cell. Pronounced salinization appears in 14%-46% of saline cells (figure 3(a)). Lower topographic gradients (dT) allow saline groundwater to intrude farther from the coast (DC) (figure 3(b)). Cells with lower hydraulic gradients (dH) are more often exposed to higher SGFs and lower thicknesses of fresh groundwater columns (TFG) (figure 3(c)). Higher hydraulic conductivity (K) increases the exposure to all three aspects of saline groundwater, illustrated by the approximately two orders of magnitude between the median hydraulic conductivity (K) in cells with moderate and pronounced aspects (figure 3(d)). The distributions of aquifer depth (D_{aqu}) in cells with moderate and pronounced aspects of saline groundwater are similar (figure 3(e)). GWR values are higher in cells with pronounced aspects of saline groundwater (figure 3(f)). The usage of thresholds other than those described in table 1 leads to similar results (figures S7 and S8), and a scatterplot version of figure 3 can be found in figure S8.

Although the influence of factors on the distribution of saline groundwater is evident, it does not show the full picture. Computing Spearman rank correlations of the factors with aspects of saline groundwater shows that weak to moderate monotonic relationships exist between most factors and aspects of saline groundwater (figure 4, text S2 provides a detailed description of figure 4).

Scatter plots of factor values and aspects of groundwater salinity indicate non-monotonic relationships between factors and aspects (see figures S9–S12), likely caused by factor interactions not captured by Spearman rank correlations. For example,

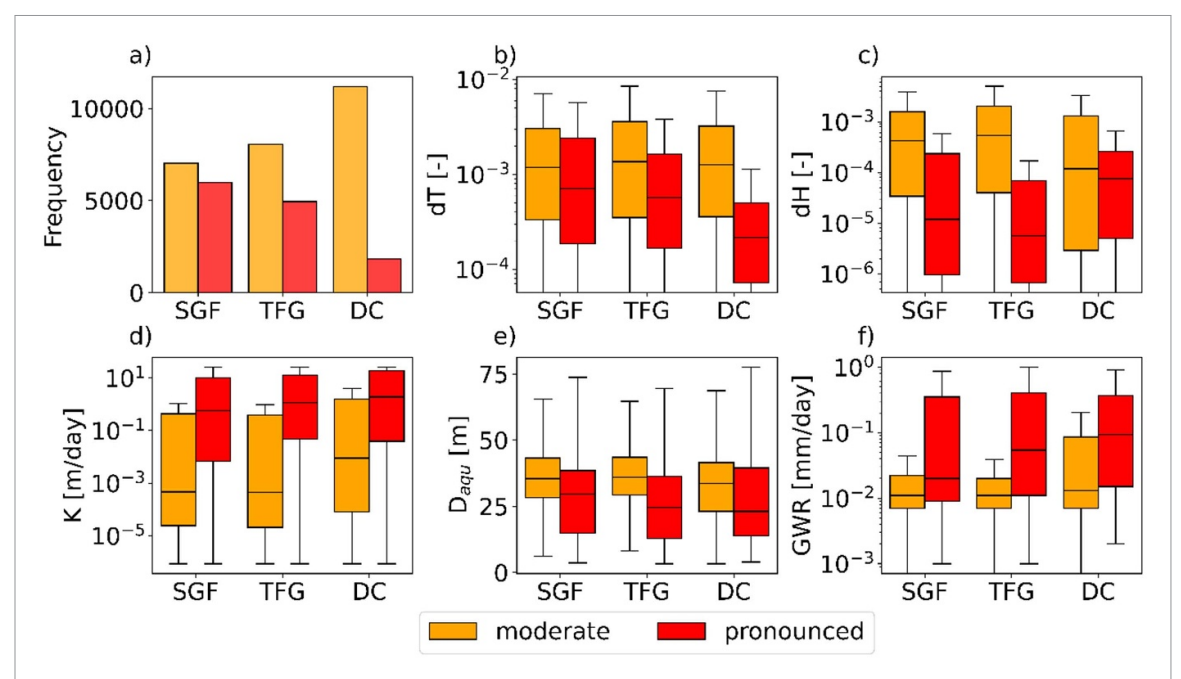


Figure 3. Subplot (a) shows the number of cells with moderate (orange) and pronounced (red) saline groundwater fraction (SGF), thickness of fresh groundwater (TFG), and distance of saline groundwater from coast (DC). Aspects of saline groundwater in cells are categorized as pronounced if SGF > 0.5, TFG < 5 m, and DC > 10 km. The remaining subplots show boxplots of cells with moderate and pronounced SGF, TFG, and DC for (b) topographic gradient (dT), (c) hydraulic gradient (dH), (d) hydraulic conductivity (K), (e) aquifer depth ($D_{\rm aqu}$), and (f) groundwater recharge (GWR).

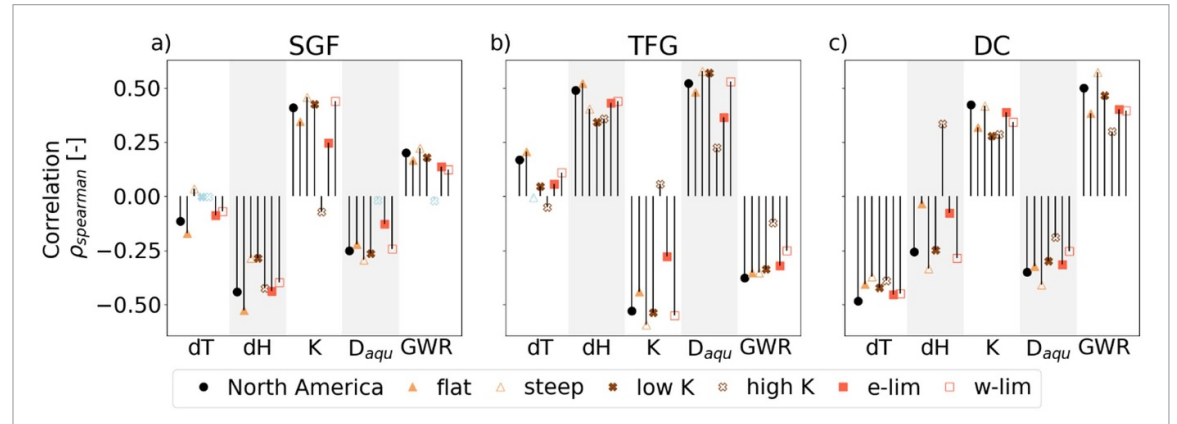


Figure 4. Spearman rank correlation of (a) saline groundwater fraction (SGF), (b) thickness of fresh groundwater column (TFG), (c) distance of saline groundwater from coast (DC) with topographic gradient (dT), hydraulic gradient (dH), hydraulic conductivity (K), aquifer depth ($D_{\rm aqu}$) and groundwater recharge (GWR). Thresholds for the delineation of flat/steep, low/high K, energy-/water-limited (e-/w-lim) regions are given in table S2. Insignificant correlations are shown in light blue. All correlations and p-values are displayed in tables S4–S6.

cells with both high hydraulic conductivity (K) and low topographic gradient (dT) are more likely to contain high fractions of saltwater while the opposite applies for cells with both low hydraulic conductivity (K) and high topographic gradient (dT). Interactions with other factors impact the results, especially in cells with intermediate hydraulic conductivity (K) and/or topographic gradient (dT), resulting in the displayed non-monotonic relationships (figures S9–S12). Overall, parameter interactions can have both positive and negative impacts on simulated aspects of groundwater salinity, depending on the factor values.

4. Discussion

Across the North American continent, we identify coastal saline groundwater, in particular in Florida (US), along the US East Coast, and in Mexico (figure S1), where issues with SWI have been reported (Barlow and Reichard 2010). Additionally, we identified regions prone to containing saline groundwater, which have hardly been studied, in Alaska (US), Nunavut (Canada), and Oaxaca (Mexico). Using simple assumptions to estimate the vulnerability towards containing saline water (see text S3), we

find that 23%/49% of the coastal area could be vulnerable due to low hydraulic/topographic gradients, while 68% of the coastal area could be vulnerable due to high hydraulic conductivities. However, parameter interactions limit the simulated area with saline groundwater to 18.6% (520 122 km²) of the coastal zone.

4.1. Model assessment

Simulating the groundwater salinity distribution on the North American coast, we find results that align with the literature, identifying aquifers with lower topographic gradient to the coast (Michael et al 2013), lower hydraulic gradient (Ferguson and Gleeson 2012), and larger aquifer thickness (Mazi et al 2013) as more vulnerable towards containing saline groundwater at shallower depth and further from the coast. Figure 3 suggests that while saline groundwater can be expected in regions with hydraulic gradients below 10^{-3} , which has been used by Ferguson and Gleeson (2012), high exposure to saline groundwater can be expected at hydraulic gradients below 10^{-4} . Of the North American coastline cells classified by Michael et al (2013) as topography-limited and thus particularly vulnerable to seawater intrusion from sea level rise, 63% contain saline water in the presented simulation. In comparison, only 47% of cells in rechargelimited regions contain saline groundwater, which indicates that topography-limited cells may already (i.e. without sea level rise) be more likely to contain saline groundwater due to their relatively flat topography.

Our results show that inland cells with hydraulic conductivity (K) above 10^{-2} m d⁻¹ are particularly vulnerable to containing saline groundwater. This is consistent with our understanding that saline groundwater can be found where hydraulic conductivity is high enough for substantial groundwater flows (e.g. Shi and Jiao 2014, Deng et al 2017, Costall et al 2020). However, the model does not contain conduits (e.g. in karstic or volcanic aquifers) or related focused groundwater exchanges between aquifers and the ocean (Kreyns et al 2020), limiting its applicability in regions with such lithology. Surprisingly, GWR values are higher in cells with pronounced aspects of saline groundwater (figure 3(f)), indicating that more saline water spreads into regions with higher GWR. Such behavior has been reported for GWR below 100 mm yr^{-1} (Michael *et al* 2013). In cells with GWR above 100 mm yr⁻¹, resilience against saline groundwater (i.e. SGF, TFG and DC) increases with increasing GWR (figure S13). However, the influence of GWR on the aspects of saline groundwater is low, potentially because topography is the main control in the underlying groundwater model (Reinecke et al

Figure S14 shows coastline observations from Thorslund and van Vliet (2020) without/with saline water and inland observations with saline water

plotted against the factor values of the cells the observations were made in. While the parameter ranges of observations are different (e.g. fewer observations within cells with hydraulic conductivity below 10⁻¹ m d⁻¹), figure S14 and S2 show similar patterns in factor values. This does not imply that the model results are correct, but shows that similarities exist between the factor ranges of regions with saline and fresh groundwater in our model and observations by Thorslund and van Vliet (2020). However, there are also strong differences between simulated and observed factor values. The median of topographic gradient (dT) in cells with observations is almost one order of magnitude smaller than in the simulated cells (observed: 0.001-0.012 vs. simulated: 0.000 27-0.0021, see tables S7 and S8). Further, the median of GWR is more than one order of magnitude larger in cells with observations than in the simulated cells (observed: 0.35-0.52 mm d⁻¹ vs. simulated: 0.013- $0.016 \,\mathrm{mm}\,\mathrm{d}^{-1}$, see tables S7 and S8). Both, model limitations and biases in observation site selection likely induce these differences.

4.2. Model limitations and assumptions

Four approximations underly the variable density routine of the groundwater model (Bakker et al 2013). First, the routine neglects resistance to flow in vertical direction within an aquifer (interpretation of the Dupuit approximation). Second, a volume balance equation is applied in the flow field calculations (following the Boussinesq-Oberbeck approximation). Third, effects of dispersion and diffusion are considered neglectable. Fourth, density inversions can only appear between aquifers (i.e. not within the same aquifer). These approximations are elemental in reducing computational cost (e.g. enabling simulation with larger and fewer model cells) to simulate coastal groundwater density at the continental scale. Nevertheless, the model's spatial resolution of 5 arcmin is very coarse for the simulation of saline groundwater. Due to the horizontal sharp interfaces, which are a consequence of the underlying approximations, saline water entering a model cell on one side may cause the horizontal interface to lift up. This shift in interface height entails that the saline water entering at one time step may be transferred further to another neighboring cell in the next simulation step, enabling saline water transport of several kilometers in just a year. Thus, the applied model likely overestimates saline groundwater movement compared to real-world dispersive transfer. Despite the likely faster movement of the saline interface, the model required 492 000 years to reach a state of very slow interface movement, indicating that the saline groundwater distribution in North America has been evolving since before the end of the last ice age, approximately 20 000 years ago. Further, the model does not account for anthropogenic actions like groundwater pumping, assumes a steady climate

and does not incorporate inland sources of salinity. Hence, the discussed model results likely do not map the actual current coastal groundwater salinity distribution. Instead, the presented model can be used to explore the natural factors controlling groundwater salinity at the coast.

4.3. Model parameter uncertainties

Global datasets were used to parameterize the groundwater model. These datasets generally incorporate considerable uncertainties. The uncertainty in hydraulic conductivity (K) from GLHYMPS 2.0 (Huscroft et al 2018) is possibly one order of magnitude (Reinecke et al 2019b). Transmissivity in aquifers with permafrost is calculated using depth to bedrock and the very low conductivity values of GLHYMPS 2.0 for permafrost regions, simplifying potentially complex ice layering of permafrost regions. Similar to hydraulic conductivity, the uncertainty in depth to bedrock is high (Shangguan et al 2017). Further, global GWR datasets show significant variance (Reinecke et al 2021). The parameterization using the discussed datasets represents a best estimate of which parameter combinations occur in North America. Since this study's focus is understanding the impacts of factor values on groundwater salinity (i.e. as opposed to mapping actual saline groundwater distribution), we evaluate parameter variability and their impact on salinity distribution (see figures 2 and 3). We do not assume that the model results reflect the real-world salinity distribution in the simulated cells, but we assess the parameter ranges for which coastal groundwater can be salinized by ocean water.

5. Conclusions

Given rapidly evolving coastal communities and growing demand for fresh groundwater in large parts of North America, improving our understanding of continental coastal groundwater salinity is pivotal. To assess the dominant controls of coastal saline groundwater occurrence and incursion at the continental scale, we have simulated variable density groundwater flow in North America until the sharp interface between fresh and saline water was stable under steady climatic forcing. Assessing the parameter values of fresh and saline cells at the coastline, we find that low topographic gradients and high aquifer depths enable saltwater to enter coastal aguifers. We show that coastline and inland cells are more vulnerable to containing saline groundwater if topographic gradients are lower and hydraulic conductivities are higher. Focusing on three aspects of coastal groundwater salinity, we show that under steady inputs, hydraulic gradient, topographic gradient, hydraulic conductivity, and aquifer depth control the salinity of coastal and inland cells. The impact of GWR seems to be limited in G³M-D. Our model results align

with previous results identifying hydraulic conductivity as control in saline groundwater distribution. With hydraulic conductivities over 10^{-2} m day⁻¹, 68% of the North American coastal zone (i.e. up to 100 km onshore an up to 100 m elevation) is, in principle, likely to carry saline groundwater. However, parameter interactions limit the simulated area with saline water to 18.6% of the North American coastal zone.

Our results suggest that North America will experience more seawater intrusion in the future, even without rising sea levels and GWR changes which were not assessed in this study. Future research should explicitly assess parameter interactions and use transient simulations to examine how changes in GWR and sea level rise impact seawater intrusion globally, particularly in regions with high hydraulic conductivities and low elevation. The resulting controls of groundwater salinity change could be used to identify potential hotspots of future salinization under climate change scenarios, providing valuable insights to decision-makers and guidance to where additional regional research might be necessary.

Data and code availability

- The code of G³M and G³M-D is available at: https://github.com/rreinecke/global-gradient-based-groundwater-model.
- The North America model of G³M-D is available at: https://github.com/EarthSystemModelling/3GM-D-NorthAmerica (includes the code of G³M-D as a git submodule).
- The elevation data by Lehner *et al* (2008) is available at: www.hydrosheds.org/products/hydrosheds.
- The groundwater recharge data by Müller Schmied *et al* (2020) is available at: https://doi.pangaea.de/ 10.1594/PANGAEA.918447
- The GLHYMPS 2.0 data (including hydraulic conductivity and effective porosity) by Huscroft et al (2018) is available at: https://borealisdata.ca/ dataset.xhtml?persistentId=doi%3A10.5683/SP2/ TTJNIU
- The CoPerm data (used to set the hydraulic conductivity of the general head boundary) by Moosdorf *et al* (2024) is available at: https://doi.pangaea.de/10.1594/PANGAEA.958901
- The depth to bedrock data (used to set aquifer depth) by Shangguan *et al* (2017) is available at: http://globalchange.bnu.edu.cn/research/dtb.jsp
- The groundwater heads and interface heights of the final time step, which are evaluated in this study, are available at: 10.5281/zenodo.13928185
- The global dataset of surface water and groundwater salinity measurements from 1980 to 2019 (Thorslund and van Vliet 2020) is available at: https://doi.pangaea.de/10.1594/PANGAEA. 913939

Data availability statement

The data that support the findings of this study are openly available at the following URL/DOI: https://zenodo.org/records/13928185.

Acknowledgments

D K is funded by Deutsche Forschungsgemeinschaft (G Z: RE 4624/1-1). R R and T W were funded by the Alexander von Humboldt Foundation in the framework of the Alexander von Humboldt Professorship endowed by the German Federal Ministry of Education and Research. HM was funded by the US National Science Foundation Coastal Critical Zone Project (EAR2012484). M B was funded by the ERC Advanced Grant Scheme (project GEOWAT No. 101019185). N M Acknowledges funding from DFG MO 2538/8-1.

Conflict of interest

None.

ORCID iDs

Daniel V Kretschmer https://orcid.org/0000-0003-0115-1268

Holly A Michael https://orcid.org/0000-0003-1107-7698

Nils Moosdorf https://orcid.org/0000-0003-2822-8261

Gualbert H P Oude Essink https://orcid.org/0000-0003-0931-6944

Marc F P Bierkens https://orcid.org/0000-0002-7411-6562

Thorsten Wagener https://orcid.org/0000-0003-3881-5849

Robert Reinecke https://orcid.org/0000-0001-5699-8584

References

- Bakker M, Schaars F, Hughes J D, Langevin C D and
 Dausman A M 2013 Documentation of the Seawater
 Intrusion (SWI2) Package for MODFLOW: U.S Geological
 Survey Techniques and Methods, Book 6 (U.S. Geological
 Survey) ch A46, p 47 (available at: https://pubs.usgs.gov/tm/6a46/)
- Barlow P M and Reichard E G 2010 Saltwater intrusion in coastal regions of North America *Hydrogeol. J.* 18 247–60
- Befus K M, Barnard P L, Hoover D J, Finzi Hart J A and Voss C I 2020 Increasing threat of coastal groundwater hazards from sea-level rise in California *Nat. Clim. Change* 10 946–52
- Cao T, Han D and Song X 2021 Past, present, and future of global seawater intrusion research: a bibliometric analysis *J. Hydrol.* **603** 126844
- Costall A R, Harris B D, Teo B, Schaa R, Wagner F M and Pigois J P 2020 Groundwater throughflow and seawater intrusion in high quality coastal aquifers *Sci. Rep.* 10 9866
- Custodio E 2010 Coastal aquifers of Europe: an overview Hydrogeol. J. 18 269–80

- Deng Y, Young C, Fu X, Song J and Peng Z-R 2017 The integrated impacts of human activities and rising sea level on the saltwater intrusion in the east coast of the Yucatan Peninsula, Mexico *Nat. Hazards* 85 1063–88
- Dieter C A, Linsey K S, Caldwell R R, Harris M A, Ivahnenko T I, Lovelace J K, Maupin M A and Barber N L 2018 Estimated use of water in the United States county-level data for 2015 (ver. 2.0, June 2018): U.S. Geological Survey data release (https://doi.org/10.5066/F7TB15V5)
- Ferguson G and Gleeson T 2012 Vulnerability of coastal aquifers to groundwater use and climate change *Nat. Clim. Change* 2 342–5
- Feth J H 1965 Preliminary map of the conterminous United States showing depth to and quality of shallowest ground water containing more than 1,000 parts per million dissolved solids: hydrologic investigations atlas HA-199 p 31
- Gnann S *et al* 2023 Functional relationships reveal differences in the water cycle representation of global water models *Nat. Water* 1 1079–90
- Harbaugh A W 2005 MODFLOW-2005, the U.S. Geological Survey modular groundwater model—the ground-water flow process *U.S. Geological Survey Techniques and Methods* 6-A16 (https://doi.org/10.3133/tm6A16)
- Henry H R 1964 Effect of dispersion on salt encroachment in coastal aquifers *U.S. Geological Survey Water-Supply Paper* Paper 1613-C pp 70–84
- Huscroft J, Gleeson T, Hartmann J and Börker J 2018 Compiling and mapping global permeability of the unconsolidated and consolidated earth: GLobal HYdrogeology MaPS 2.0 (GLHYMPS 2.0) *Geophys. Res. Lett.* 45 1897–904
- Jasechko S, Perrone D, Seybold H, Fan Y and Kirchner J W 2020 Groundwater level observations in 250,000 coastal US wells reveal scope of potential seawater intrusion *Nat. Commun.* 11 3229
- Ketabchi H, Mahmoodzadeh D, Ataie-Ashtiani B and Simmons C T 2016 Sea-level rise impacts on seawater intrusion in coastal aquifers: review and integration *J. Hydrol.* **535** 235–55
- Kreyns P, Geng X and Michael H A 2020 The influence of connected heterogeneity on groundwater flow and salinity distributions in coastal volcanic aquifers J. Hydrol. 586 124863
- Lehner B, Verdin K and Jarvis A 2008 New global hydrography derived from spaceborne elevation data *EOS Trans. Am. Geophys. Union* 89 93–94
- Manivannan V and Elango L 2019 Seawater intrusion and submarine groundwater discharge along the Indian coast Environ. Sci. Pollut. Res. 26 31592–608
- Mazi K, Koussis A D and Destouni G 2013 Tipping points for seawater intrusion in coastal aquifers under rising sea level Environ. Res. Lett. 8 014001
- Michael H A, Russoniello C J and Byron L A 2013 Global assessment of vulnerability to sea-level rise in topography-limited and recharge-limited coastal groundwater systems *Water Resour. Res.* 49 2228–40
- Moosdorf N, Tschaikowski J, Kretschmer D and Reinecke R 2024 A global coastal permeability dataset (CoPerm 1.0) *Sci. Data* 11 893
- Müller Schmied H *et al* 2020 The global water resources and use model WaterGAP v2.2d—standard model output [dataset] *PANGAEA* (https://doi.org/10.1594/PANGAEA.918447)
- Post V E A, Eichholz M and Brentführer R 2018 *Groundwater Management in Coastal Zones* (Bundesanstalt für
 Geowissenschaften und Rohstoffe (BGR)) p 107
- Reilly T E, Dennehy K F, Alley W M and Cunningham W L 2008 Ground-water availability in the United States: U.S Geological Survey Circular No. 1323 p 70
- Reinecke R *et al* 2021 Uncertainty of simulated groundwater recharge at different global warming levels: a global-scale multi-model ensemble study *Hydrol. Earth Syst. Sci.* 5 787–810
- Reinecke R et al 2024 Uncertainty in model estimates of global groundwater depth Environ. Res. Lett. 19 114066

- Reinecke R, Foglia L, Mehl S, Herman J D, Wachholz A, Trautmann T and Döll P 2019a Spatially distributed sensitivity of simulated global groundwater heads and flows to hydraulic conductivity, groundwater recharge, and surface water body parameterization *Hydrol. Earth Syst. Sci.* 23 4561–82
- Reinecke R, Foglia L, Mehl S, Trautmann T, Cáceres D and Döll P 2019b Challenges in developing a global gradient-based groundwater model (G³M v1.0) for the integration into a global hydrological model *Geosci. Model Dev.* 12 2401–18
- Richardson C M, Davis K L, Ruiz-González C, Guimond J A, Michael H A, Paldor A, Moosdorf N and Paytan A 2024 The impacts of climate change on coastal groundwater *Nat. Rev. Earth Environ.* 5 100–19
- Sawyer A H, David C H and Famiglietti J S 2016 Continental patterns of submarine groundwater discharge reveal coastal vulnerabilities *Science* 353 705–7
- Shangguan W, Hengl T, Mendes J J, Yuan H and Dai Y 2017 Mapping the global depth to bedrock for land surface modeling *J. Adv. Model. Earth Syst.* **9** 65–88

- Shi L and Jiao J J 2014 Seawater intrusion and coastal aquifer management in China: a review Environ. Earth Sci. 72 2811–9
- Thorslund J and van Vliet M T H 2020 A global dataset of surface water and groundwater salinity measurements from 1980–2019 Sci. Data 7 231
- Weedon G P, Balsamo G, Bellouin N, Gomes S, Best M J and Viterbo P 2014 The WFDEI meteorological forcing data set: WATCH Forcing Data methodology applied to ERA-Interim reanalysis data *Water Resour. Res.* 50 7505–14
- Werner A D and Simmons C T 2009 Impact of sea-level rise on sea water intrusion in coastal aquifers *Ground Water* 47 197–204
- Wilson S and Fischetti T 2010 Coastline Population Trends in the United States: 1960–2008: Population Estimates and Projections (U.S. Census Bureau)
- Zamrsky D, Oude Essink G H P and Bierkens M F P 2024 Global impact of sea level rise on coastal fresh groundwater resources *Earth's Future* 12 e2023EF003581